## Title

A simplified computational model of possible hydrodynamic interactions between respiratory and swimming-related water flows in labriform-swimming fishes



## Journal

Bioinspiration & Biomimetics, 16(3)

## ISSN

1748-3182

## Authors

Leung, David B
Eldredge, Jeff D
Gordon, Malcolm S

## Publication Date

2021-05-01

## DOI

10.1088/1748-3190/abdab7

Peer reviewed

Bioinspiration & Biomimetics



# A simplified computational model of possible hydrodynamic interactions between respiratory and swimming-related water flows in labriform-swimming fishes

To cite this article before publication: David B. Leung *et al* 2021 *Bioinspir. Biomim.* in press https://doi.org/10.1088/1748-3190/abdab7

# A simplified computational model of possible hydrodynamic interactions between respiratory and swimming-related water flows in labriform-swimming fishes

David B. Leung[1], Jeff D. Eldredge[1], Malcolm S. Gordon[2*]

[1] Mechanical & Aerospace Engineering, University of California, Los Angeles, CA, 90095, USA

[2] Ecology & Evolutionary Biology, University of California, Los Angeles, CA, 90095, USA

[*]Author for correspondence (msgordon@ucla.edu)

Key Words: CFD, labriform-swimming, swimming performance, maneuverability, hydrodynamics, respiratory water flow

Running title: **Respiratory water flows affect fish swimming**

**Abstract**

Hydrodynamic interactions in bony fishes between respiratory fluid flows leaving the opercular openings and simultaneous flows generated by movements of downstream pectoral fins are both poorly understood and likely to be complex. Labriform-swimming fishes that swim primarily by moving only their pectoral fins are good subjects for such studies. We performed a computational fluid dynamics (CFD) investigation of a simplified two-dimensional model of these interactions based on previously published experimental observations of both respiratory and pectoral fin movements under both resting and slow steady swimming conditions in two similar labriform swimmers: the bluegill sunfish (*Lepomis macrochirus*) and the largemouth bass (*Micropterus salmoides*). We carried out a parametric study investigating the effects that swimming speed, strength of opercular flow, and phase difference between the pectoral fin motion and the opercular opening and closing have on the thrust and side slip forces generated by the pectoral fins during both the abduction and adduction portions of the fin movement cycle. We analyzed pressure distributions on the fin surface to determine physical differences in flows with and without opercular jets. The modeling indicates that complex flow structures emerge from the coupling between the opercular jets and vortex shedding from pectoral fins. The jets from the opercular openings appear to exert significant influence on the forces generated by the fins; they are potentially significant in the maneuverability of at least some labriform swimmers. The numerical simulations and the analysis establish a framework for study of these interactions in various labriform swimmers in a variety of flow regimes. Similar situations in groups of fishes using other swimming modes should also be investigated.

**Introduction**

Three major bodily functions of fishes are primarily based on hydrodynamic processes: feeding (especially suction feeding), respiration and swimming. This paper is a first approximation computational modeling (CFD) study of an aspect of the fluid dynamic connections between respiration and swimming that has until now received minimal attention. It has three primary goals:

1) To serve as a case study of these connections in a specific functional group of bony fishes, the labriform swimmers.
2) To present a simplified two-dimensional computational model that establishes a proof of concept that fluid dynamic interactions between breathing and swimming in

labriform swimmers are complex and probably significant both for locomotion and maneuverability.

3) To provide a partial foundation for future experimental and computational studies of comparable interactions in many other groups of fishes in addition to labriform swimmers.

The research literature relating to each of the functions describes in detail many aspects of these processes (Dabiri, 2019; Dabiri and Gordon, 2017; Higham et al., 2006; Lauder and Tytell, 2006; Sfakiotakis et al., 1999; Van Wassenbergh, 2015; Webb, 2006; Westneat, 2006). Hughes modeled the respiratory process as a periodic dual pump system that results in water leaving the opercular openings due to pressure differences between the opercular cavities and the ambient fluid (Hughes, 1960; Lauder, 1984; Brainerd and Ferry-Graham, 2006; Wegner and Graham, 2010). Evans et al. (2005) reviewed the anatomy and multiple functions of fish gills, including their function in respiration. An important aspect missing from this literature is explicit discussion of the hydrodynamic processes involved in the interactions between excurrent

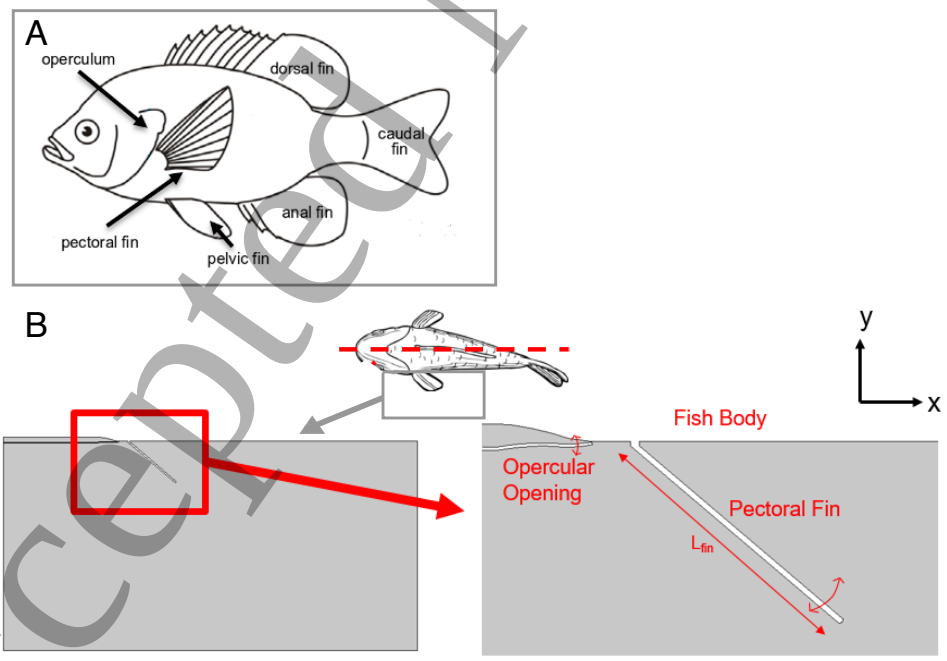


*Fig. 1 (A) External anatomy of a labriform swimming fish (Bluegill Sunfish), adapted from (Lauder 2006). (B) Two-dimensional simulation geometry, carried out in the frontal plane, depicted as the gray box adjacent to the fish.*

respiratory flows and flows related to swimming. This paper is a beginning effort at filling this information gap.

Many living bony fishes have their pectoral fins located closely posterior to their opercular openings, as seen in Fig. 1A. This proximity makes highly probable significant complex hydrodynamic interactions between excurrent respiratory water flows and flows generated by moving pectoral fins. Fishes swimming in labriform modes generate most of their thrust from pectoral fin motions. Those motions also are often central to both swimming performance and maneuverability (Drucker and Jensen, 1996; Drucker et al., 2006; Gibb et al., 1994; Jones et al., 2007; Lauder et al., 2006; Mittal et al., 2006; Mussi et al., 2002; Ramamurti et al., 2002; Shoele and Zhu, 2010).

Here we report a computational fluid dynamics (CFD) study of these flows based on the properties of two experimentally well-studied labriform-swimming species of centrarchid fresh-water fishes, the bluegill sunfish (*Lepomis macrochirus*) and the large-mouth bass (*Micropterus salmoides*) (Lauder 1984; Lauder et al 2006; Mittal et al 2006). Rather than attempt to capture the complex three-dimensional motion of the fin and the associated fluid dynamics, we focus on a simplified model that distills the most crucial aspects of this interaction: a two-dimensional geometry (in the frontal plane), consisting of a single rigid fin undergoing symmetric abduction and adduction just downstream of a simple oscillatory model of the opercular opening. Though this model cannot be used to accurately predict the forces generated by actual fish, it can provide a phenomenological understanding of the flow in the vicinity of the opercular jet and the fin as well as reasonable estimates for the degree of flow interaction. In particular, by comparing the forces and pressure distributions generated on the simplified fin with and without the influence of the jet, we can draw conclusions as to whether the interaction is significant and merits further study.

Fishes swim and maneuver over wide ranges of speeds and flow conditions. Accordingly, we investigated appropriate ranges of parameter values. The results, especially trends observed in key parameters, indicate that excurrent respiratory flows significantly affect forces generated by moving pectoral fins in at least labriform swimmers like those we modeled. Further experimental and computational studies of similar interactions that must occur in other lineages of fishes that swim in other swimming modes are needed.

The results demonstrate three important points:

1) Flows leaving the opercula interact with flows around the adjacent pectoral fins in many complex ways.

2) Forces generated by these flows are both complex and significant in magnitude.
3) These interactions are probably important for both swimming performance and maneuverability of these fishes.

## Materials and Methods

### *Model geometry*

Our objective in this study is to assess the degree to which the opercular jet influences the forces generated by the fin in a representative model of labriform swimming, for a wide variety of physical parameters. Several simplifying choices were made in order to ensure computational efficiency of the model for exploring a large parametric space while still retaining the basic mechanisms of this mode of swimming. Fig. 1B depicts the geometry of the computational model. The pectoral fin of a generic labriform-swimming fish was modeled as a rigid, straight, and two-dimensional (in the frontal plane) flat plate. The approximate dimensions of the pectoral fin as well as the location of the opercular opening and other important parameters were chosen to roughly match those of a bluegill sunfish. The dimensions of the baseline numerical simulation, described in more detail below, as well as those of the bluegill sunfish (Lauder et al., 2006) and largemouth bass (Lauder et al., 1984), are shown in Table 1. The geometry and motion were assumed to be symmetric about the mid-sagittal plane, so that only the left side of the fish was modeled.

The pectoral fin was rotated in a prescribed sinusoidal oscillatory motion about a fixed pivot axis adjacent to the fish body, shown in Fig. 2. The opercular opening was modeled as a small gap at the end of a long narrow channel separated from the main fluid region by a thin wall. The gap opens and closes via a prescribed sinusoidal rotation of the end portion of a thin wall, about a pivot at the end of the straight section of the channel, also depicted in Fig. 2. For both the fin and the opercular opening motions, the angle with respect to the positive x axis was described by

$$\theta_z(t) = \theta_o + \theta_r \sin(2\pi f t + \varphi), \qquad (2)$$

where $\theta_o$ is the mean angle, $f$ is the frequency (in Hz), $t$ is time (in seconds), $\varphi$ is the phase, and $\theta_r$ is the amplitude. A positive phase difference between the two motions corresponds to the pectoral fin oscillation leading that of the opercular opening, as illustrated in Fig. 2. Note that both the fin and the opercular opening were prescribed to oscillate with the same frequency, representative of synchronized respiration and pectoral fin motions often observed in labriform

swimming. This frequency as well as the mean angle and amplitude for each motion are reported in Table 1.

The inlet of the channel leading to the opercular opening was modeled with a constant and uniform inlet pressure ($\Delta P$). We note that, while the maximum width of the channel and opening were chosen to approximately match a fully opened gill cover, the length of the channel leading into the opercular opening is not chosen based on physiology. The flow generated in the channel is approximately a quasi-steady Poiseuille flow, and it exits from the opercular opening with a fully-developed velocity profile. The prescribed oscillatory opening and closing of the opercular opening coupled with a fixed pressure difference mimics the oscillatory pressures generated in the buccal cavities of fishes. The flow rate through the channel is linearly proportional to the pressure difference and proportional to the fourth power of the channel width. Thus, oscillating either the pressure or the opening width can produce an oscillatory velocity leaving the gills. Modulations of the width, as we employ here, have their effect amplified approximately by a factor of four on perturbations to the flow rate, so it is unnecessary to modulate the pressure, as well.

Because of the simplifications described here, we do not expect that the forces predicted by the model (interpreted per unit height in the dorsal-ventral direction) will faithfully reproduce those observed on a pectoral fin of a real fish. This is especially true during the upstroke (abduction) portion of the pectoral fin movement cycle since a rigid fin produces drag during this phase; in contrast, the pectoral fin of an actual labriform swimmer deforms during this recovery in order to produce thrust throughout the entire abduction and adduction cycle (Mittal et al., 2006). The simplified model is designed to capture the primary abduction and adduction of the fin, which we argue is sufficiently representative of labriform swimming for demonstrating the

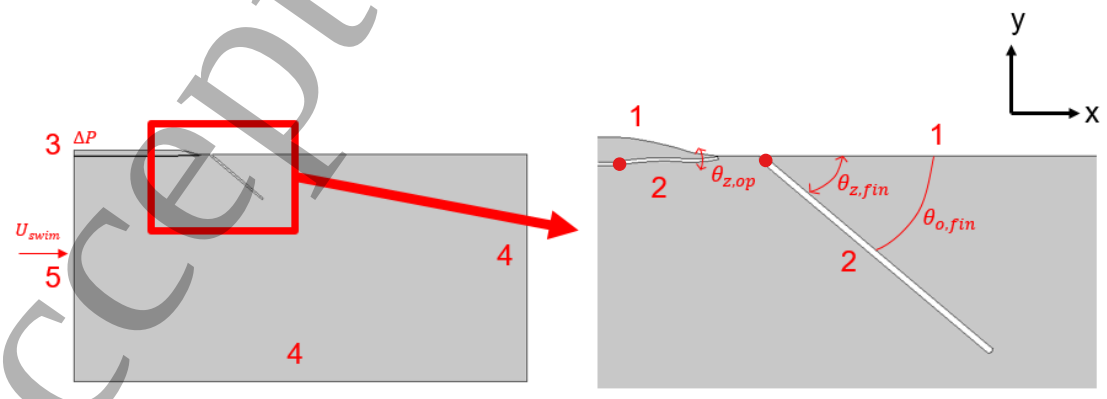


*Fig. 2: Boundary conditions for simulation. 1: Wall, 2: Moving wall (oscillatory), 3: Pressure inlet, 4: Pressure outlet, 5: Velocity inlet. Red circles on right panel denote the pivots of the plate and opercular opening.*

leading-order influence of the opercular jet on the fin's generated forces. It should also be noted that the interaction between the pectoral fin and respiratory flow occurs mainly at the base of the pectoral fin, which remains relatively rigid.

*Numerical simulations and boundary and initial conditions*

Navier-Stokes simulations were conducted with COMSOL Multiphysics. We set up a time dependent, incompressible, laminar flow solver, based on backward-differentiation second-order time stepping in finite element formulation, with the parameters outlined below. COMSOL Multiphysics solves the coupled Navier-Stokes and continuity equations,

$$\rho \frac{D\vec{u}}{Dt} = -\nabla P + \mu \nabla^2 \vec{u}, \quad (7)$$

$$\nabla \cdot \vec{u} = 0, \quad (8)$$

under the conditions outlined above, where $\vec{u}$ is the velocity vector and $P$ is the pressure.

The five boundary conditions used for this simulation are depicted in Fig. 2 in the supplemental material. The fish body was modeled as a rigid wall on which the no-slip and no-flow-through conditions were enforced. The pectoral fin and opercular opening were modeled as walls of prescribed motion, described above, also with the no-slip and no-flow-through conditions enforced. To accommodate the moving boundaries, the built-in Arbitrary Lagrangian-Eulerian re-meshing scheme in COMSOL Multiphysics was implemented to automatically re-mesh the geometry during specified motions of the fin and opercular channel.

All of the other boundaries of the computational domain were positioned far from the fin and opercular opening. The right and lower boundaries of the computational domain were treated as outlets of uniform pressure. The left boundary of the computational domain was treated as a velocity inlet, with incoming flow normal to the boundary specified with the specific swimming speed ($U_{swim}$) for the fish. It should be noted that the size of the computational domain, which is shown in the left-hand panel in Fig. 1B (and S2 in the supplemental material), is more compact (around 4 fin lengths across) than those typically used in external flow simulations of a moving fin (~20-30 lengths). We chose to use this more compact domain in order to achieve the computational efficiency needed for exploring a wide range of parameters. The consequence of the smaller domain is the potential for influence from the boundaries. However, we reason that such influence is essentially irrelevant, given our principal objective of

Table 1: Parameters used in the study, compared with reference values for fish

| Parameter | Bluegill Sunfish (Lauder et al., 2006) | Bass (Lauder et al., 1984) | Baseline simulation |
|---|---|---|---|
| $\rho$ | 1000 kg m$^3$ | 1000 kg m$^3$ | 1000 kg m$^3$ |
| $\mu$ | $10^{-3}$kg m$^{-1}$ s$^{-1}$ | $10^{-3}$kg m$^{-1}$ s$^{-1}$ | $10^{-3}$ kg m$^{-1}$ s$^{-1}$ |
| $\Delta P$ | N/A | 50 Pa | 2 Pa |
| $f_{fin}$ | 2.17 s$^{-1}$ | 1 s$^{-1}$ | 0.1 s$^{-1}$ |
| $f_{op}$ | N/A | N/A | 0.1 s$^{-1}$ |
| $L_{fin}$ | 0.04 m | 0.04 m | 0.045 m |
| $U_{swim}$ | 0.16 m s$^{-1}$ (1.1 lengths/s$^{-1}$) | N/A | 0.0113 m s$^{-1}$ (.077 lengths/ s$^{-1}$) |
| $\theta_{o,fin}$ | N/A | N/A | -22.5° |
| $\theta_{r,fin}$ | N/A | N/A | 17.5° |
| $\theta_{o,op}$ | N/A | N/A | -17.5° |
| $\theta_{r,op}$ | N/A | N/A | -17.5° |
| $Re_{fin\,tip} = \frac{\rho f_{fin} L_{fin}^2}{\mu}$ | 3470 | 1600 | 203 |
| $Re = \frac{\rho U_{swim}\, L_{fin}}{\mu}$ | 6400 | N/A | 506 |
| Dimensionless pressure, $\frac{\Delta P}{\rho f_{fin}^2 L_{fin}^2}$ | N/A | 31.3 | 98.8 |
| $St = \frac{f_{fin} L_{fin}}{U_{swim}}$ | 0.543 | N/A | 0.4 |

exhibiting the differences with and without an opercular jet in a simplified model. The influence of nearby boundaries does not affect the conclusions drawn from this comparative study.

The initial condition was chosen as zero flow. The simulation was run until the pressure distribution along the fin reached a stationary periodic state.

*Flow parameters*

We modeled the main flow characteristics based on typical values for a bluegill sunfish and largemouth bass, as seen in Table 1. The relevant physical parameters are $\rho$, the density of water; $U_{swim}$, the fish swimming speed; $L_{fin}$, the length of the pectoral fin; $\mu$, the viscosity of water; $f_{fin}$, the pectoral fin beat frequency; and $\Delta P$, the specified pressure difference along the channel leading to the opercular opening. For each case, density and viscosity were chosen to be approximately that of seawater.

To achieve dynamical similarity with a typical labriform-swimming fish, the dimensionless parameters that should be matched are the swimming Reynolds number, *Re*,

$$Re = \frac{\rho U_{swim} L_{fin}}{\mu}, \quad (3)$$

which assesses the ratio of inertial to viscous forces in the water; the Strouhal number,

$$St = \frac{f_{fin} L_{fin}}{U_{swim}}, \quad (4)$$

which represents the relative speeds of the tip of the fish fin and that of the fish itself; and the dimensionless pressure difference in the opercular channel,

$$\Delta\widetilde{P} = \frac{\Delta P}{\rho f_{fin}^2 L_{fin}^2}, \quad (5)$$

which determines the speed of the opercular jet relative to that of the fish fin. In some cases the fish swimming speed was set to zero, in which case the Strouhal and Reynolds numbers are individually irrelevant, but their product represents an alternative Reynolds number based on the fish fin's tip speed,

$$Re_{fin\ tip} = \frac{\rho f_{fin} L_{fin}^2}{\mu}. \quad (6)$$

This fin Reynolds number is relevant for all cases explored and measures the relative roles of inertial and viscous effects in the flow generated by the moving fin.

The Strouhal number was explored over a range typical of fish swimming, as was the dimensionless pressure driving the opercular jet; the values of these parameters are reported in Table 2. We kept the fin Reynolds number fixed at 203 throughout. This value is approximately one order of magnitude smaller than those observed in largemouth bass (1600) and bluegill sunfish (3500). Though this lower Reynolds number limits the size of the smallest length scales of features that emerge in the flow, the two-dimensional geometry used in this study would artificially constrain the behavior of many of these higher-Reynolds-number flow features if they

Table 2: Ratio of Swimming Velocity for Given St to Spatially-Averaged Velocity Through Opercular Opening at $\Delta\tilde{P} = 100$

| **St** | **$U_{swim}/U_{avg}$** |
|---|---|
| 0.1 | 1.970 |
| 0.15 | 1.313 |
| 0.175 | 1.125 |
| 0.2 | 0.985 |
| 0.25 | 0.788 |
| 0.3 | 0.657 |
| 0.4 | 0.493 |
| 0.6 | 0.328 |

were allowed to emerge. Based on earlier simulations of the pectoral fin mechanics (Mittal et al., 2006), neither the absence of these features, nor the somewhat stronger role of viscous effects at this lower Reynolds number, are expected to impact the main objective of the study, to explore the interaction between the opercular jet and the fin.

*Baseline simulation*

For the baseline simulation, we chose flow parameters to approximately match a slow moving labriform swimmer breathing normally. As discussed above, the fin Reynolds number was fixed at approximately 200 for all simulations. The Strouhal number was set in this initial simulation to 0.4. These choices resulted in the model fish pectoral fin oscillating at a frequency of 0.1 Hz and a swimming speed of 0.01125 m $s^{-1}$, as reported in Table 1. We modeled the pectoral fin to start open with initial angle -40° and rotate through a total angle of 35°, toward the body and back, as seen in Fig. 2. These correspond to a mean angle $\theta_{0,fin} = -22.5°$ and amplitude $\theta_{r,fin} = 17.5°$, used in all simulations.

We modeled the opercular opening to oscillate in phase with the pectoral fin at 0.1 Hz. The opercular opening started closed (0°) and rotated through angle -35° away from the body and back, corresponding to $\theta_{o,op} = -17.5°$ and $\theta_{r,op} = -17.5°$. To ensure that the pectoral fin and opercular opening motions were in phase with each other, the initiation of the motion of the opercular opening was delayed until it matched with the pectoral fin motion. It is useful to note that the maximum velocity of the tip of the fin in these conditions was $0.0086$ m/s, or $1.9 f_{fin} L_{fin}$.

The pressure difference ($\Delta P$) in the opercular channel was chosen as 2 Pa, resulting in a dimensionless pressure of $\Delta\tilde{P} = 100$, somewhat higher (but on the same order of magnitude) than that of a largemouth bass, as seen in Table 1. A larger value was chosen to offset the pressure lost to resistance in the leading channel. The frequency used for this comparative calculation was the frequency of motion of the largemouth bass's opercular opening rather than its pectoral fin beat frequency since the latter frequency was not available.

We carried out a mesh convergence study on this baseline simulation as well as on cases at two other pressure differences. The results of the convergence study, including the mesh used for all reported cases, are shown in Figs. S2 to S4 in the supplemental material. The adaptive time step was set to a maximum of 0.001 s throughout, based on a similar (unreported) convergence study. Videos of contour plots of vorticity for the baseline simulation can be found in the supplemental material.

*Parametric study*

The parameters used in the baseline simulation are approximate for a slow moving fish. We performed a parametric study varying several key parameters of the flow, including the pressure of the opercular jets, the phase difference between the motions of the pectoral fin and the opercular opening, and the Strouhal number, to encompass a wide variety of fish species and flow regimes. The varying parameters are reported in Table S1 of the supplemental material. Note that, as Strouhal number varies, the swimming Reynolds number varies in inverse proportion so that their product (the fin Reynolds number) remains fixed. This parametric study will show trends in thrust and side slip in response to changes in these parameters.

*Comparison with control case with no opercular jet*

We were most interested in how the opercular jet flow affects both the thrust and side slip forces generated by the pectoral fin. To determine these forces, we numerically integrated pressure along both sides of the fin (as well as the tip) using a trapezoidal rule and found each component of the force from

$$\vec{F} = -\int P\vec{n}dS, \tag{9}$$

where $\vec{F}$ is the force vector, $P$ is the pressure, $\vec{n}$ is the outward normal vector, and d$S$ is the arc length around each point of the fin. The force in the negative $x$ direction was interpreted as thrust and the force in the negative $y$ direction as side slip.

Note that this equation only accounts for the pressure contribution to the force. The viscous contributions were not included primarily for the reason that, at the reduced Reynolds number and two-dimensional context of this study, their importance would be exaggerated in the overall balance with pressure. The reported force time series data were filtered with a five-point moving average.

To assess the degree to which the opercular jet affects the flow, all cases were compared with a corresponding control case with no opercular jet flow ($\Delta\tilde{P} = 100$) but with all other parameters identical. The deviation of any case from this control case was quantified with the root mean squared (RMS) difference between the pectoral fin forces:

$$RMS = \sqrt{\frac{\sum_{i=1}^{n}(F_{i,\text{control}} - F_i)^2}{n}}, \tag{10}$$

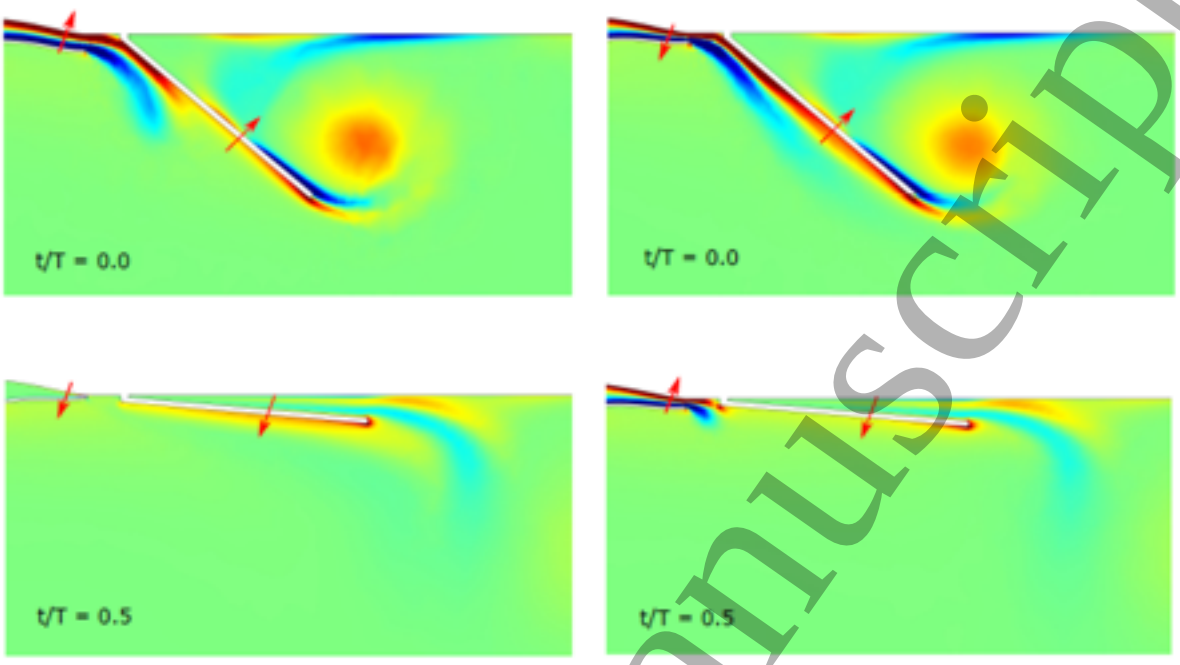


*Fig. 3: Vorticity surface plots at the beginning and middle of the pectoral fin movement cycle for phase 0° (Left) and 90° (Right). Arrows denote direction of movement as t/T increases. The vorticity contours in this plot and all subsequent plots range between -150 and 150 (normalized by frequency).*

where *n* is the number of time steps used in the calculation. Only the last cycle of the pectoral fin motion was included in this calculation, after it was ensured that the flow had reached a stationary periodic state. The RMS difference for each force component (thrust and sideslip) was computed separately and normalized by the inertial scaling, $\rho f_{fin}^2 L_{fin}^3/2$.

## Results

### *Characteristics of the flow*

The flow created by the oscillation of the pectoral fin and from the opercular opening comprises four main flow structures, as can be observed in the snapshots in Fig. 3 of the baseline case and a case with phase of 90°. The first flow structure is the vortex shedding created at the tip of the pectoral fin when it oscillates back and forth. This is characterized by a vortex with positive (*i.e,* counter-clockwise) sense during the abduction (downstroke) phase and a weaker vortex with negative sense during the adduction (upstroke) phase. These can also be seen clearly in the videos included in the supplemental material. Both of these vortices dissipate as they travel downstream.

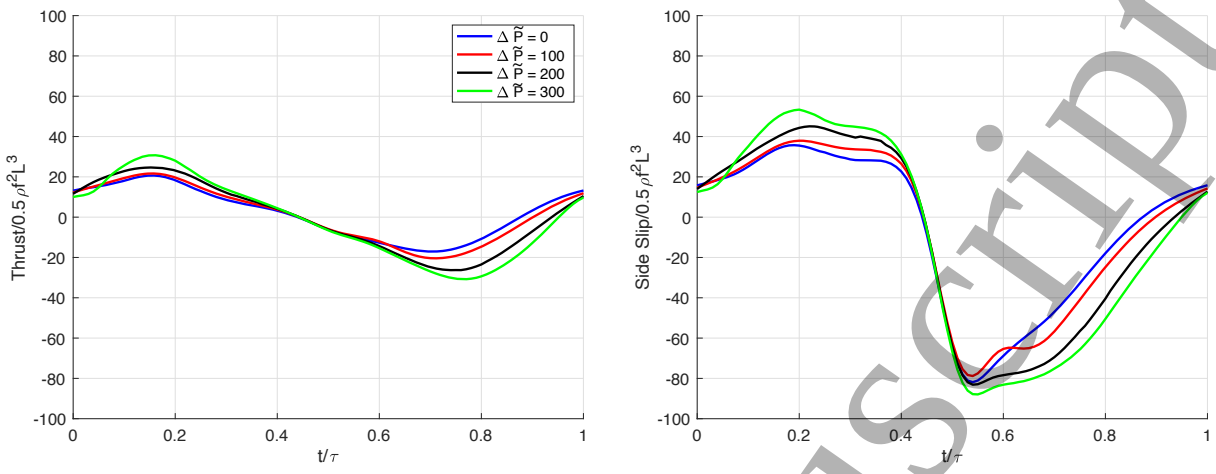


*Fig. 4: Thrust (Left) and side slip forces (Right) over 1 pectoral fin oscillation period, varying pressure in opercular jet. Swimming speed is zero and phase difference is 0°.*

The second main flow structure is a jet flow issuing from the opercular opening and following along the pectoral fin. This flow structure can also be seen in the videos in the supplemental material. After its initial encounter with the base of the fin, this jet tends to flow away from the body, following the fin's moving contour.

Another important flow structure is the boundary layer that develops along the pectoral fin and along the fish body both in front of and behind the pectoral fin. As St decreases (and swimming Reynolds number increases), the boundary layer at the fin body in front (to the left) of the pectoral fin becomes stronger. When St decreases to 0.1, this boundary layer creates enough vorticity to interact strongly with the pectoral fin.

A final characteristic of this flow occurs in the interaction between the pectoral fin and fish body. When the pectoral fin goes through its adduction phase, it squeezes fluid out of the space between the pectoral fin and fish body. On the other hand, fluid flows back into this space when the pectoral fin goes through its abduction phase, creating a boundary layer of reverse sign. Later in this abduction phase, the vortex generated at the fin tip induces this reverse boundary layer to separate from the fish body, exhibited by the light blue vorticity directly aft of the fin at $t/T = 0$ in Fig. 3.

*Effect of varying the strength of the opercular jet*

In this section we explore the effect of varying the pressure difference in the opercular channel on the interaction between the opercular jet and the pectoral fin. All cases here have no swimming speed (St = ∞) and 0° phase difference between the pectoral fin and opercular

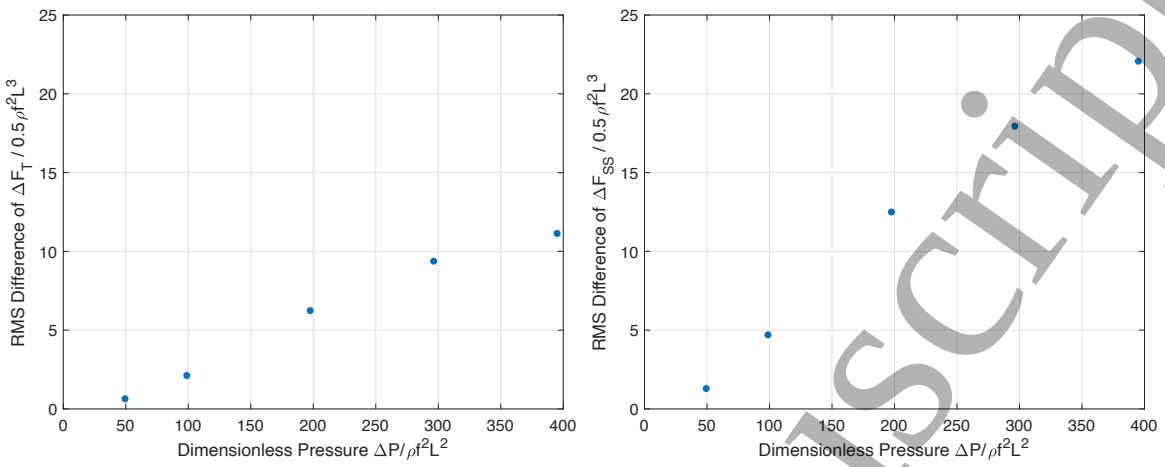


*Fig. 5: RMS differences of dimensionless thrust (Left) and side slip (Right) over 1 pectoral fin oscillation period, for varying pressure in opercular jet*

opening motion. To provide a better sense of the effect of these changes in pressure difference, we show in Table S2 of the supplemental material the spatially-averaged velocity through the opercular channel at the beginning of the pectoral fin movement cycle ($t/T$ = 0.0, when the opercular opening has its maximum area) for each case. This velocity increases nearly linearly with pressure difference, but starts to saturate at large pressure as non-linear inertial effects in the fluid become significant.

Fig. 4 shows the time histories of the nondimensional thrust and side slip forces on the pectoral fin for three different choices of opercular pressure difference, $\Delta\tilde{P}$, including the control case with no opercular flow. It is clear from these results that the opercular jet has a significant effect on both force components, particularly during the abduction phase (the second half of the period). Its effect is to generally enhance the basic behavior observed during both the adduction and abduction phases, for example, increasing positive thrust during adduction and increasing drag (decreasing negative thrust) during the abduction stroke.

This effect is apparent in Fig. 5, which shows the RMS differences from control for the thrust and side slip forces for several choices of $\Delta\tilde{P}$. There is an approximately linear relationship between both RMS differences and the dimensionless $\Delta\tilde{P}$. Increasing $\Delta\tilde{P}$ by 50 increases dimensionless thrust by about 1.48 and increases dimensionless side slip by about 3.4. Thus, increasing flow through the opercular opening has a larger effect (greater than twice) on increasing side slip forces than it does on increasing thrust. The force results in this figure are expressed in inertial scaling units, $\rho f_{fin}^2 L_{fin}^3/2$. For reference, the RMS values of the force components themselves in the control case, expressed in the same inertial units, are 12.0 and

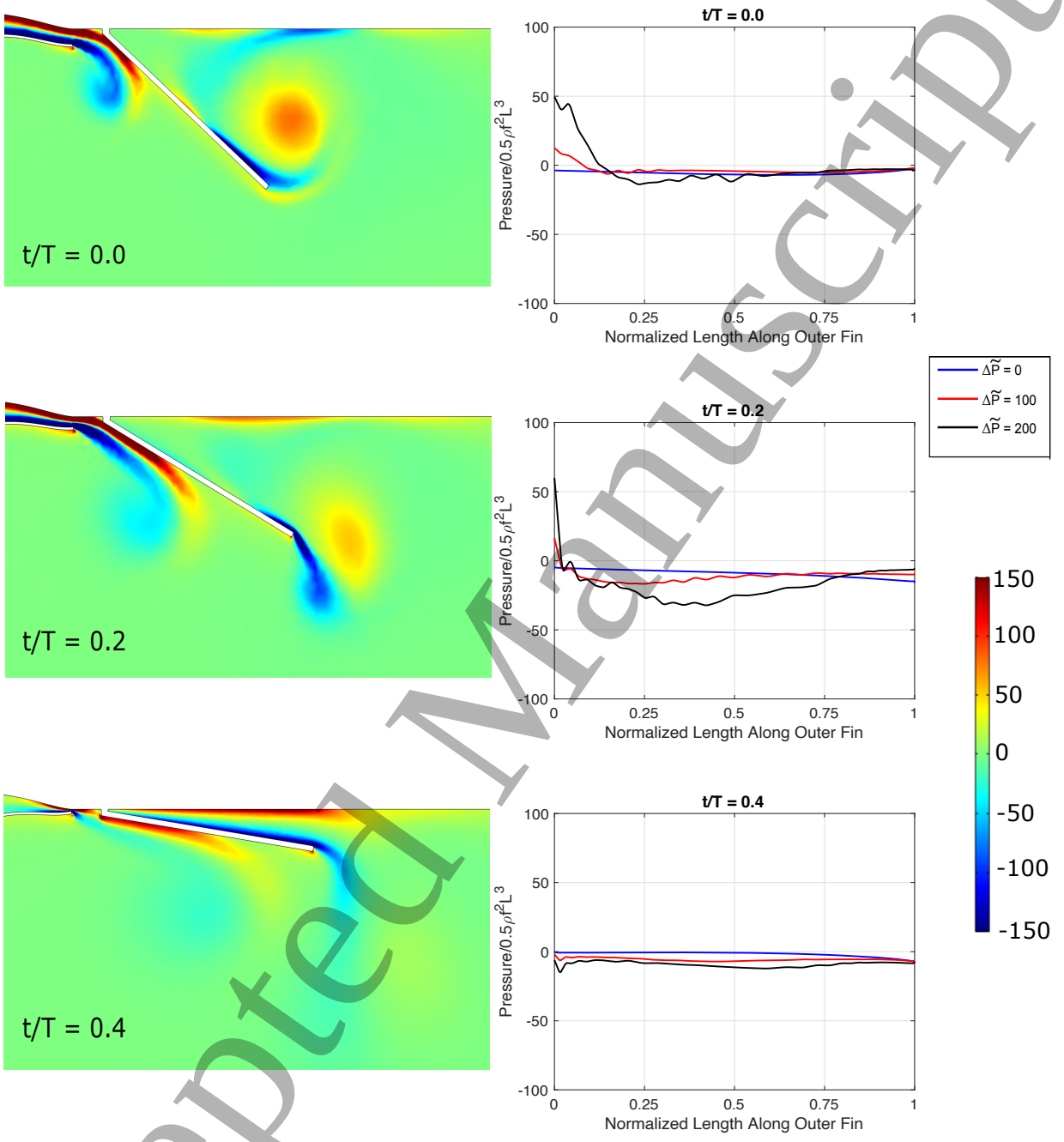


*Fig. 6: Vorticity contour plots (Left) and pressure distribution plots along the outward side of the fin (Right) at every fifth of the pectoral fin oscillation period from t/T = 0.0 to t/T = 0.4, varying opercular pressure. Vorticity contour plots are for $\Delta\tilde{P} = 100$, 0° phase difference*

38.3, so the RMS differences are of the same order of magnitude, particularly at the largest opercular pressures.

To explain the differences in each case, the pressure distribution along the outward-facing side of the pectoral fin is plotted in Fig. 6 at every fifth of the oscillation period, for

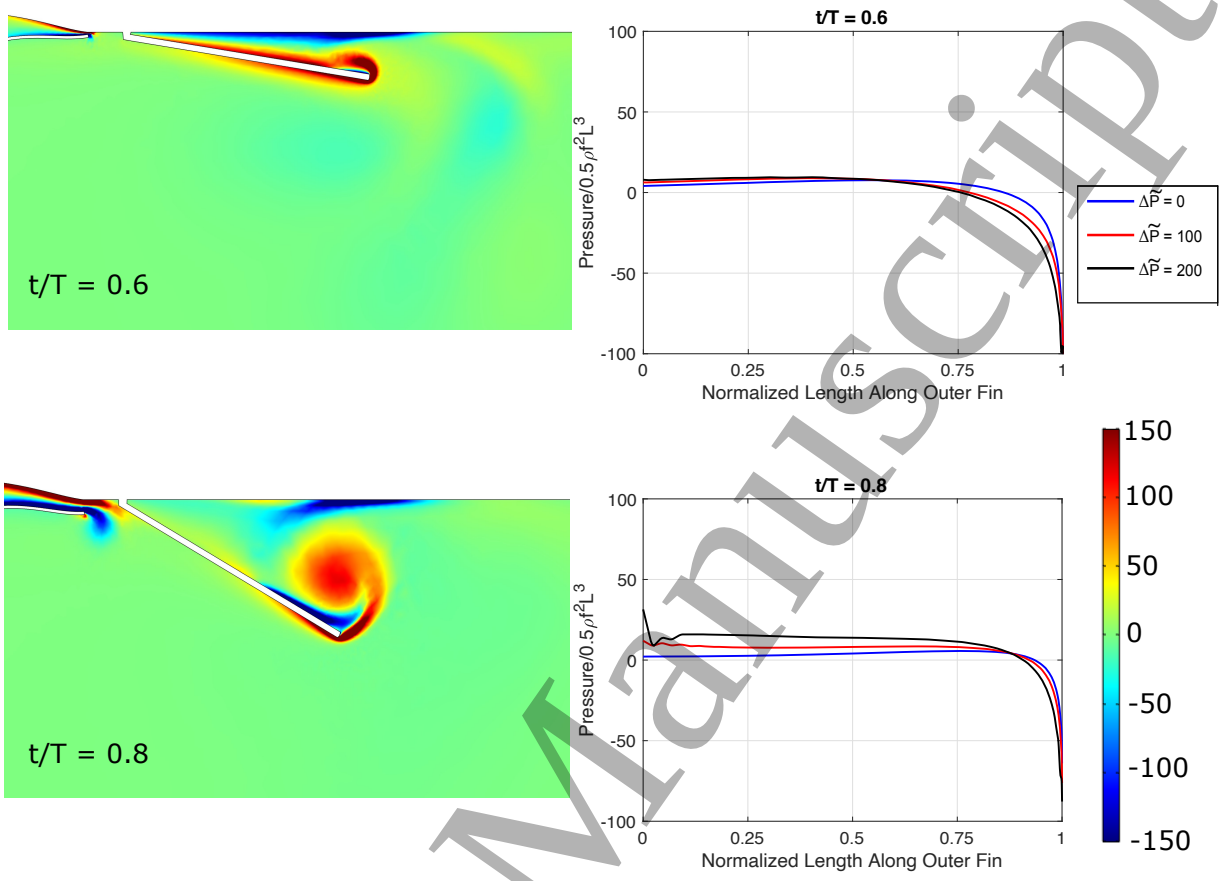


*Fig. 6 (cont'd): Vorticity contour plots (Left) and pressure distribution plots along the outward side of the fin (Right) at every fifth of the pectoral fin oscillation period from t/T = 0.6 and t/T = 0.8, varying opercular pressure. Vorticity contour plots are for $\Delta\tilde{P} = 100$, 0° phase difference*

different choices of $\Delta\tilde{P}$. For these plots, 0 on the horizontal axis denotes the base of the pectoral fin while 1 represents the tip. Only the pressure on the outward portion of the fin was plotted since the opercular jet only interacts with this side. Positive pressure is associated with force acting toward the fin; negative pressure is suction. For comparative purposes, these distributions are shown alongside the vorticity contour plots at the corresponding times.

The results of Fig. 6 show that, throughout the adduction and abduction phases, the opercular jet has a large effect on the pressure distribution along the pectoral fin, particularly near the base of the fin (position 0). This is expected since the jet flow from the opercular opening predominantly interacts with and affects the pectoral fin near its base. It should also be observed that the pressure due to the jet changes sign along the fin. For example, at early times in the cycle, it is positive (thrust-reducing) near the base and negative (thrust-enhancing) further

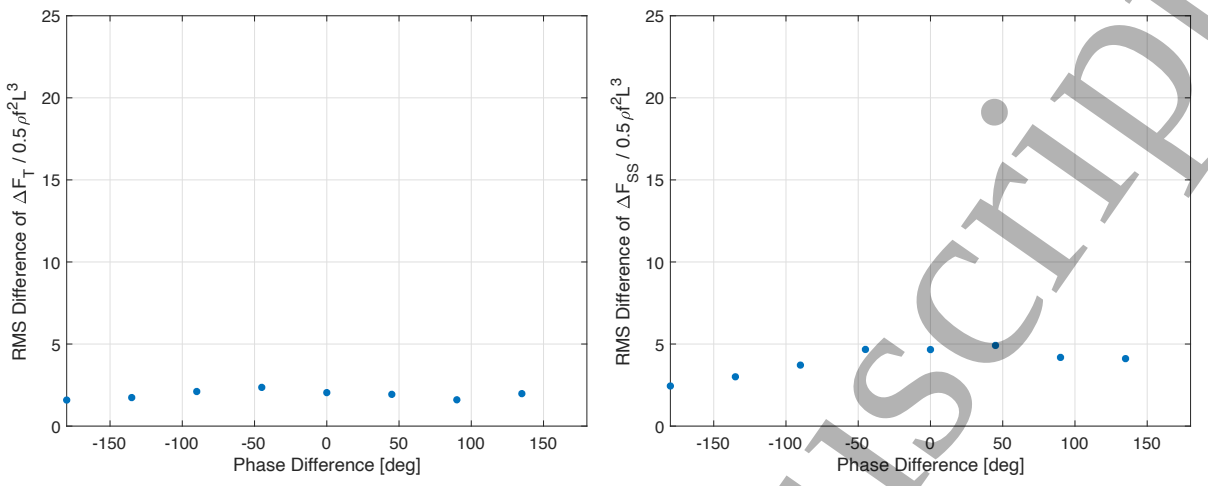


*Fig. 7: RMS differences of dimensionless thrust (Left) and side slip (Right) over 1 pectoral fin oscillation period, varying phase difference*

along the fin. The small region of positive pressure near the base is indicative of the stagnation of the jet flow on the fin, while the negative suction is due to a Bernoulli effect from the enhanced velocity in the jet as it follows the contour of the fin.

In the second half-stroke, the sign of the pressure attributable to the jet changes from negative to positive over most of the fin, enhancing the drag and the negative side slip on the fin. This positive pressure is not associated with an obvious flow structure. However, by this point in the cycle, the opercular jet generated during the first half-stroke has pinched off from the opening and the jet's tail has traversed the fin. This tail is followed by a slightly larger pressure, distributed over most of the fin.

It is notable that, for much of the cycle, the differences in pressure distribution due to the jet are weak and unconcentrated, but their integrated effect remains significant, as exhibited by the RMS force differences.

*Effect of varying phase difference*

Here, we vary the phase difference between the pectoral fin and opercular opening motions to explore the effect of the timing of these two oscillations on the interaction. For all of these cases, $\Delta\tilde{P} = 100$ and St = ∞. The control case is once again taken as the no-opercular-jet case ($\Delta\tilde{P} = 0$) with St = ∞.

The plots of RMS difference of thrust and side slip relative to the control case are shown in Fig. 7. Most notable in these plots is the relatively small changes of RMS difference with varying phase difference. There remains a mild effect on the sideslip force difference, with the

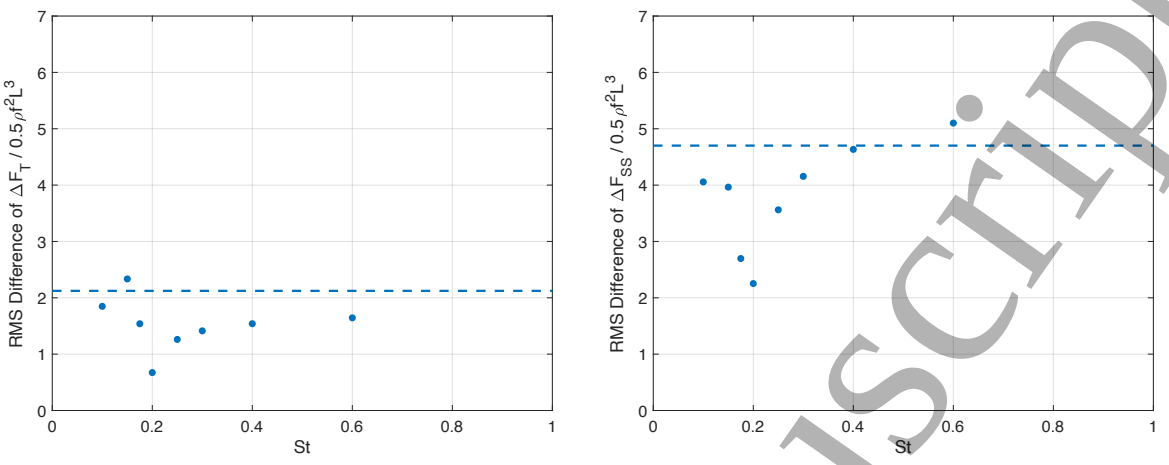


*Fig. 8: RMS differences of dimensionless thrust (left) and side slip (right) over 1 pectoral fin oscillation period, varying St*

greatest influence apparent between -45° and 45° phase difference. However, the net effect of the opercular jet on the fin appears to be relatively insensitive to the phase difference between the motions of the fin and opercular opening. Pressure distribution and vorticity contour plots (included in the supplemental material) show that, while the jet flow's interaction with the fin is shifted in time by the changing phase difference, most of the aspects of this interaction that influence the force are unaffected by this shift.

*Effect of varying Strouhal number*

Finally, in this section, the interactions between opercular jet and fin are explored for different swimming speeds, captured by varying the Strouhal number. All of these cases have 0° phase difference and $\Delta\tilde{P} = 100$. Table 2 reports the ratio of swimming speed to the peak spatially-averaged velocity of the jet issuing from the opercular opening at each Strouhal number. For each case, its corresponding control case is taken as the no-opercular-flow case ($\Delta\tilde{P} = 0$) at the same Strouhal number.

The RMS differences between each case and its corresponding control case are depicted in Fig. 8. With varying St, both components exhibit interesting non-linear trends, distinctly centered at St = 0.2, where the RMS difference is smallest. It is important to note that at this Strouhal number the swimming speed matches the peak jet velocity. In other words, the relative speed between the jet and the surrounding mass of fluid is smallest for this Strouhal number. Thus, the effect of the opercular jet on the fin is weakest at this Strouhal number.

For higher St cases, the RMS difference increases then levels off as St increases, eventually approaching the RMS difference for zero swimming speed (St = ∞). Interestingly, this

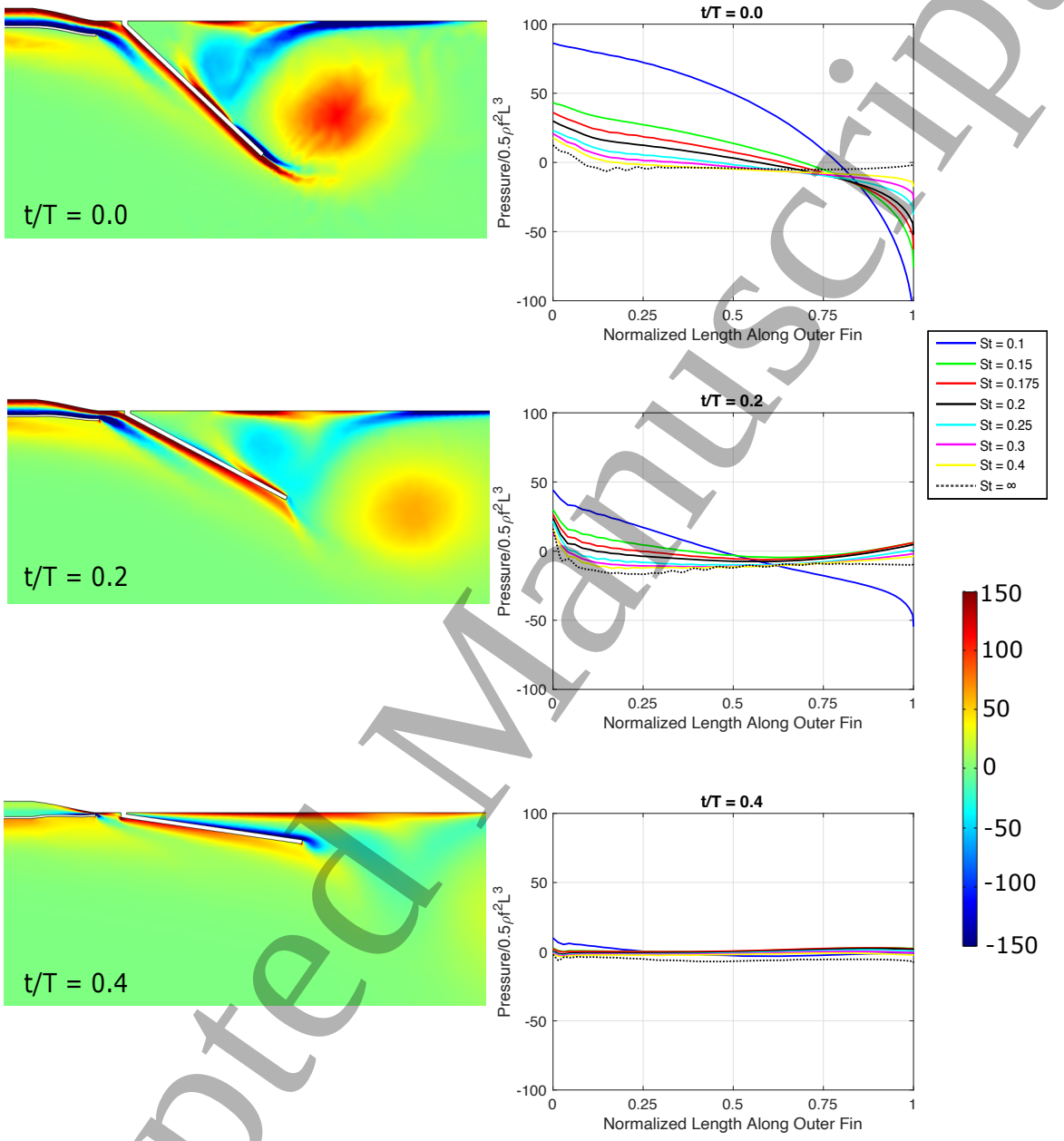


*Fig. 9: Vorticity contour plots (Left) and pressure distribution plots along the outward side of the fin (Right) at every fifth of the pectoral fin oscillation period from t/T = 0.0 to t/T = 0.4, varying St. Vorticity contour plots are for $\Delta\tilde{P} = 100$, 0° phase difference, St = ∞*

asymptotic RMS difference is nearly achieved at small St number (St < 0.2), as well. For such cases, the opercular jet is slower than the bulk flow near the opercular opening compared to the control case.

Snapshots of the pressure distribution plots for several Strouhal numbers can be found in Fig. 9, with the corresponding vorticity surface plots at St = 0.15 shown for reference.

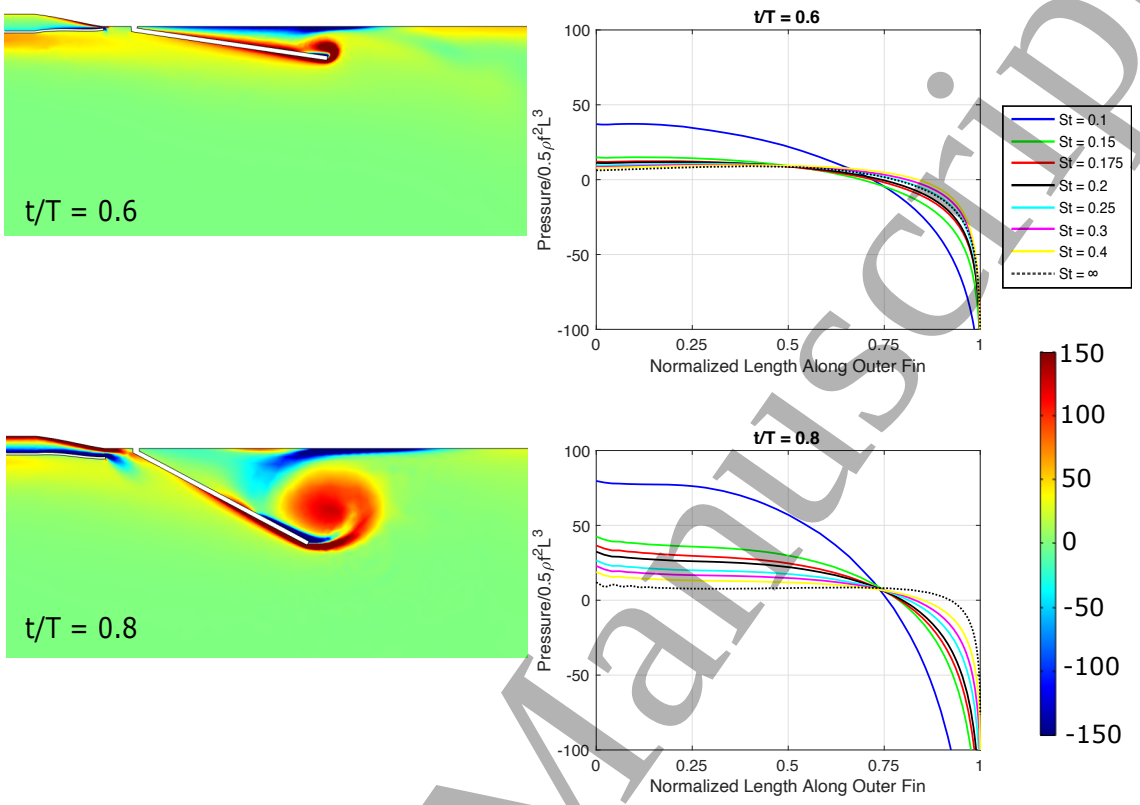


*Fig. 9 (cont'd): Vorticity contour plots (Left) and pressure distribution plots along the outward side of the fin (Right) at every fifth of the pectoral fin oscillation period from t/T = 0.6 and t/T = 0.8, varying St. Vorticity contour plots are for $\Delta\tilde{P} = 100$, 0° phase difference, St = ∞*

Decreasing St from infinity tends to increase the pressure at the base of the fin, but decrease the pressure (create more suction) at the tip of the fin. In general, the cases of St above 0.1 have very similar trends in the pressure distribution. The St = 0.1 case exhibits the same basic distributions, but stands apart from the others in its magnitude. This is probably due to the fact that the boundary layer from the fish body in front of the pectoral fin is strong enough at St = 0.1 that it now interacts with the pectoral fin itself.

## Discussion

We simulated the flows about a simplified first-principles-based two-dimensional rigid model of the gill opercula and the pectoral fins of one morphotype of labriform-swimming fish as those fishes breath and move through the water at low speeds. We performed a parametric study of these flows varying key parameters (ΔP, phase, and Strouhal number). Flows from the opercular openings during respiratory cycles create important and complex flow structures. We compared the thrust and side slip forces generated for each parametric study case with a

control case without opercular flow. Flows from the opercular openings generally enhance the time-varying forces generated during fin strokes.

Effects of the opercular jets were significant on both force components, but more so on the side slip. Furthermore, these effects increased nearly linearly with the pressure differences driving the flows through the opercular openings. Based on the computed relationships between these pressure differences and peak flow rates in the jets the effects are also proportional to flow rates in the opercular jets. Notably, the timing between the motions of the fins and those of the opercular openings did not significantly alter the effects.

The relative speeds of movements of the fins to the swimming speeds of the fish, determined by the Strouhal number, had significant influence on the effects of the opercular jets. Most notably when the velocities of the flows exiting the opercular openings are nearly matched with swimming speeds, effects of the jets on the fins are greatly diminished. The effects are gradually recovered as the Strouhal number increases, corresponding to comparatively slower swimming or faster fin motion. Interestingly, the effect is also strong at Strouhal numbers for which the jet is slower than the swimming speed.

The flow structures generated at the opercular opening, which coalesces into a starting jet, interacts with the downstream fin in a manner that is reminiscent of the interactions between tandem pairs of dorsal fins (Akhtar et al., 2007). However, we do not see evidence here of the vortex pairing that underpins the thrust augmentation in the trailing fin of a tandem pair.

These results indicate that, while at least one morphotype of labriform-swimming fish can potentially use respiratory flows to enhance their swimming speeds, we think they are more likely to either use these flows to help them maneuver or to reject side force disturbances while swimming. While fishes cannot immediately increase opercular flows at any given instant, even moderate-speed opercular jets generate non-negligible forces compared to movements of the pectoral fins alone.

Experimental approaches to refining and verifying these results will be neither simple nor easy. Flow visualization studies involving three-dimensional digital particle imaging velocimetry (DPIV) will be essential. Obtaining usable data will be challenges for coming generations of students of fish swimming.

## Conclusion

This study is both a case study and a proof of concept. It has shown, using a simple first-principles-based two-dimensional computational model, that the interactions between respiratory flows and the kinematics of movements of the pectoral fins can have small but significant effects on the thrust and side slip forces generated in at least one morphotype of labriform-swimming fishes as they move through the water. These interactions involve three principal processes: the initial impacts of the excurrent jets on the bases of the pectoral fins; the suctions exerted on the fins as the jets flow over them; and the excess pressures that trail the pinched-off jets as they leave the tips of the fins.

In real fishes the depth dimension will affect these interactions in multiple substantive ways. One of the more important ways is likely in the balances between the momenta of the opercular jets and those generated by the fins. These interactions will also undoubtedly be modified by deformations of the fins. We will not speculate on whether these complexities may enhance or detract from the results observed in this simplified model. We conclude that these interactions should not be neglected and deserve further study.

The design spaces occupied by fishes swimming partly or primarily in the labriform mode are complex. The dozens of evolutionary lineages include a wide range of adult body sizes and varied body forms ranging from strongly laterally compressed to near circular cross-sections; there also are forms varying from relatively short-bodied to quite elongate. Pectoral fin shapes vary widely from relatively short and fan-shaped to elongate and falcate; the fins vary from relatively stiff to very flexible. Positions of the insertions of pectoral fins downstream of opercular openings vary substantially; the angles of those insertions vary from near horizontal to near vertical. The two centrarchid species we modeled are both relatively short-bodied, laterally compressed, have flexible fins, have pectoral insertions close to opercular openings and have near-vertical insertions. It is probable that the many combinations and permutations of these anatomical features found in other lineages, when studied either experimentally or computationally, will yield a diversity of interesting and possibly useful discoveries relating to both the hydrodynamics and the energetics of their swimming. It is also probable that comparable complexities of interactions between excurrent respiratory flows and flows around fish bodies will be found in many fish lineages using other swimming modes.

## List of symbols and abbreviations

RMS Root Mean Squared

| | |
|---|---|
| St | Strouhal Number |
| Re | Reynolds Number |
| $\theta_r$ | Amplitude of rigid-body rotation |
| f | Frequency |
| $\varphi$ | Phase lead of fin oscillation to opercular opening |
| $t$ | Time |
| $\rho$ | Density of Water |
| $U_{swim}$ | Swimming Speed |
| $L_{fin}$ | Length of the pectoral fin |
| $\mu$ | Viscosity of water |
| $f_{fin}$ | Pectoral fin beat frequency |
| $\Delta P$ | Specified pressure difference to drive the opercular jet flow |
| $\vec{u}$ | Velocity vector |
| $\nabla P$ | Pressure gradient |
| $\vec{F}$ | Force vector |
| P | Pressure |
| $\vec{n}$ | Normal vector |
| $F_i$ | Force generated by the pectoral fin at time *i* for the corresponding case |
| n | Number of time steps used |
| $U_{avg}$ | Average spatial velocity through opercular opening |

**Competing Interests**

The authors declare no competing interests.

**Funding**

We gratefully acknowledge support for this work from a Faculty Research Grant of the UCLA Academic Senate.

## References

**Akhtar, I., Mittal, R., Lauder, G. V. and Drucker, E.** (2007). Hydrodynamics of a biologically inspired tandem flapping foil configuration. *Theor. Comput. Fluid Dyn.* **21**, 155-170.

**Bozkurttas, M., Mittal, R., Dong, H., Lauder, G.V. and Madden, P.** (2009). Low-dimensional models and performance scaling of a highly deformable fish pectoral fin. *J. Fluid Mech.* **631**, 311-342.

**Brainerd, E. L. and Ferry-Graham, L. A.** (2006). Mechanics of respiratory pumps. In *Fish Biomechanics* (ed. R.E. Shadwick and G. V. Lauder), pp. 1-28. San Diego: Elsevier Academic Press, Inc.

**Dabiri, J. O.** (2019). Landmarks and frontiers in biological fluid dynamics. *Physical Review Fluids* **4**: 110501.

**Dabiri, J. O. and Gordon, M. S.** (2017). Swimming. In *Animal Locomotion: Physical Principles and Adaptations* (ed. M. S. Gordon, R. Blickhan, J. O. Dabiri and J.J. Videler), pp. 29-92. Boca Raton: CRC Press.

**Dong, H., Bozkurttas, M., Mittal, R., Madden, P. and Lauder, G.V.** (2010). Computational modeling and analysis of the hydrodynamics of a highly deformable fish pectoral fin. *J. Fluid Mech.* **645**, 345-373.

**Drucker, E.G. and Jensen, J.S.** (1996). Pectoral Fin Locomotion in the Striped Surfperch II. Scaling Swimming Kinematics and Performance at a Gait Transition. *J. Exp. Biol.* **199**, 2243-2252.

**Drucker, E. G., Walker, J. A. and Westneat, M. W.** (2006). Mechanics of pectoral fin swimming in fishes. In *Fish Biomechanics* (ed. R.E. Shadwick and G.V. Lauder), pp. 369-423. San Diego: Elsevier Academic Press, Inc.

**Evans, D.H., Piermarini, P.M. and Choe, K.P.** (2005). The Multifunctional Fish Gill: Dominant Site of Gas Exchange, Osmoregulation, Acid-Base Regulation, and Excretion of Nitrogenous Waste. *Physiol. Rev.* **85**, 97-177.

**Gibb, A.C., Jayne, B.C. and Lauder, G.V.** (1994). Kinematics of Pectoral Fin Locomotion in the Bluegill Sunfish *Lepomis macrochirus*. *J. Exp. Biol.* **189**, 133-169.

**Higham, T.E., Day, S.W. and Wainwright, P.C.** (2006). Multidimensional analysis of suction feeding performance in fishes: fluid speed, acceleration, strike accuracy and the ingested volume of water. *J. Exp. Biol.* **209**, 2713-2725.

**Hughes, G.M.** (1960). A comparative study of gill ventilation in marine telosts. *J. Exp. Biol.* **37**, 28-45.

**Jones, E.A., Jong, A.S. and Ellerby, D.J.** (2008). The effects of acute temperature change on swimming performance in bluegill sunfish *Lepomis macrochirus*. *J. Exp. Biol.* **211**, 1386-1393.

**Jones, E.A., Lucey, K.S. and Ellerby, D.J.** (2007). Efficiency of labriform swimming in the bluegill sunfish (*Lepomis macrochirus*). *J. Exp. Biol.* **210**, 3422-3429.

**Korsmeyer, K.E., Steffensen, J.F. and Herskin, J.** (2002). Energetics of median and paired fin swimming, body and caudal fin swimming, and gait transition in parrotfish (*Scarus schlegeli*) and triggerfish (*Rhinecanthus aculeatus*). *J. Exp. Biol.* **205,** 1253-1263.

**Lauder, G.V.** (1984). Pressure and Water Flow Patterns in the Respiratory Tract of the Bass (*Micropterus salmoides*). *J. Exp. Biol.* **113**, 151-164.

**Lauder, G.V., Madden, P., Mittal, R., Dong, H. and Bozkurttas, M.** (2006). Locomotion with flexible propulsors: I. Experimental analysis of pectoral fin swimming in sunfish. *Bioinsp. Biomim.* **1**, S25-S34.

**Lauder, G. V. and Tytell, E. D.** (2006). Hydrodynamics of undulatory propulsion. In *Fish Biomechanics* (ed. R. E. Shadwick and G. V. Lauder), pp. 425-468. San Diego: Elsevier Academic Press, Inc.

**Liu, G., Ren, Y. Dong, H., Akanyeti, O., Liao, J.C. and Lauder, G.V.** (2017). Computational analysis of vortex dynamics and performance enhancement due to body-fin and fin-fin interactions in fish-like locomotion. *J. Fluid Mech.* **829**, 65-88.

**Mittal, R., Dong, H., Bozkurttas, M., Lauder, G.V. and Madden, P.** (2006). Locomotion with flexible propulsors: II. Computational modeling of pectoral fin swimming in sunfish. *Bioinsp. Biomim.* **1**, S35-S41.

**Mussi, M., Summer, A.P. and Domenici, P.** (2002). Gait transition speed, pectoral fin-beat frequency and amplitude in *Cymatogaster aggregata*, *Embiotoca lateralis* and *Damalichthys vacca*. *J. Fish Biol.* **61**, 1282-1293.

**Ramamurti, R., Sandberg, W.C., Löhner, R., Walker, J.A. and Westneat, M.W.** (2002). Fluid dynamics of flapping aquatic flight in the bird wrasse: three-dimensional unsteady computations with fin deformation. *J. Exp. Biol.* **205**, 2997-3008.

**Sfakiotakis, M., Lane, D.M. and Davies, B.C.** (1999). Review of Fish Swimming Modes for Aquatic Locomotion. *IEEE J. Oceanic Eng.* **24**, 237-252

**Shoele. K. and Zhu, Q.** (2010). Numerical simulation of a pectoral fin during labriform swimming. *J. Exp. Biol.* **213**, 2038-2047.

**Van Wassenbergh, S.** (2015). Solution Strategy to Include the Opening of the Opercular Slits in Moving-Mesh CFD Models of Suction Feeding. *Integr. Comp. Biol.* **55**, 62-73.

**Webb, P.W.** (1984). Body Form, Locomotion and Foraging in Aquatic Vertebrates. *Amer. Zool.* **24**, 107-120.

**Webb, P. W.** (2006). Stability and maneuverability. In *Fish Biomechanics* (ed. R. E. Shadwick and G. V. Lauder), pp. 281-332. San Diego: Elsevier Academic Press, Inc.

**Wegner, N.C. and Graham, J.B.** (2010). George Hughes and the history of fish ventilation: From Du Verney to the present. *Comp. Biochem. Physiol. Part A* **157,** 1-6.

**Westneat, M. W.** (2006). Skull biomechanics and suction feeding in fishes. In *Fish Biomechanics* (ed. R. E. Shadwick and G. V. Lauder), pp.29-75. San Diego: Elsevier Academic Press, Inc.